

Additive manufacturing of stellite 6 superalloy by direct laser metal deposition – Part 1: Effects of laser power and focal plane position

Moradi, M., Ashoori, A. & Hasani, A.

Author post-print (accepted) deposited by Coventry University's Repository

Original citation & hyperlink:

Moradi, M, Ashoori, A & Hasani, A 2020, 'Additive manufacturing of stellite 6 superalloy by direct laser metal deposition – Part 1: Effects of laser power and focal plane position', Optics and Laser Technology, vol. 131, 106328.

<https://dx.doi.org/10.1016/j.optlastec.2020.106328>

DOI 10.1016/j.optlastec.2020.106328

ISSN 0030-3992

Publisher: Elsevier

NOTICE: this is the author's version of a work that was accepted for publication in Optics and Laser Technology. Changes resulting from the publishing process, such as peer review, editing, corrections, structural formatting, and other quality control mechanisms may not be reflected in this document. Changes may have been made to this work since it was submitted for publication. A definitive version was subsequently published in Optics and Laser Technology, 131, (2020) DOI: 10.1016/j.optlastec.2020.106328

© 2020, Elsevier. Licensed under the Creative Commons Attribution-NonCommercial-NoDerivatives 4.0 International <http://creativecommons.org/licenses/by-nc-nd/4.0/>

Copyright © and Moral Rights are retained by the author(s) and/ or other copyright owners. A copy can be downloaded for personal non-commercial research or study, without prior permission or charge. This item cannot be reproduced or quoted extensively from without first obtaining permission in writing from the copyright holder(s). The content must not be changed in any way or sold commercially in any format or medium without the formal permission of the copyright holders.

This document is the author's post-print version, incorporating any revisions agreed during the peer-review process. Some differences between the published version and this version may remain and you are advised to consult the published version if you wish to cite from it.

Additive Manufacturing of Stellite 6 Superalloy by Direct Laser Metal Deposition – Part 1: Effects of Laser Power and Focal Plane Position

Mahmoud Moradi^{1,2}, Ali Ashoori^{1,2}, Arman Hasani²

1-Department of Mechanical Engineering, Faculty of Engineering, Malayer University, Malayer, Iran.

2-Laser Materials Processing Research Center, Malayer University, Malayer, Iran.

Abstract:

This paper surveys the additive manufacturing (AM) of stellite 6 Cobalt-based superalloy by direct laser metal deposition method (DLMD) experimentally. In the present research, a coaxial nozzle head coupled with a continuous fiber laser with a maximum power of 1 kW was used. The purpose of the current research is investigating two strategies for DLMD additive manufacturing; the first one was changing the focal plane position of the laser beam inside the powder stream, 4mm above and 4mm below the powder concentration plane, and the second one was investigating the variation of the laser power (100-300 W). Some characteristics such as the geometrical dimensions (height and width), microhardness profile, grain size, and microstructure of the 3D printed wall samples were studied. The stability of the additively manufactured wall in terms of height was investigated. The results indicated that locating the focal plane position above the substrate, led to the more interaction area between the laser beam and powder stream and caused the higher height of the AMed wall. Results showed that when the focal plane position is near to the powder stream focus, the more stability will be obtained. By locating the laser spot point 2 mm above the powder concentration plane, better stability achieved. Increasing the laser power has a reverse effect on the height and stability: the more laser power, the higher height of the AMed wall, and the less stability observed. Results indicate that the laser power of 100 and 150 W has the highest height stability. The trend of changes in the grain size of the samples shows that the beginning and the end of the AMed wall are more significant than the sample's center and the trend of the microhardness variation is in a reverse regime of the grain size. Also, the average grain size will be increased when the laser power increased. The largest and the smallest average grain size are 3.13 μm and 2.11 μm for the highest and the lowest laser power, respectively.

Keywords: Additive Manufacturing; Direct Laser Metal Deposition; Stellite 6 Cobalt-Base Superalloy; Dimensional Stability; Grain size; Hardness.

1. Introduction:

The Additive Manufacturing (AM) process is considered as new technology and a revolution in production industries. Significant research has been done to understand the process and to prove and improve its capabilities [1]. This method has great potentials to make pieces with very complex shapes. It is also able to use different types of powder for the manufacturing of the part. Additive manufacturing or what has just been mentioned as 3D printers, is a type of manufacturing in which the component is completed in a layer-to-layer manner, and the final shape of the piece is made. The thickness of the layers is smaller, the dimensional precision of the pieces and the final surface quality are more precise. The advantages of additive manufacturing method compared to the other manufacturing methods is that there is no need to design a mold and there is no molding process for manufacturing of a component, while the layers are added to each other through G-codes, even the complex desired shape of a part can be produced with high dimensional accuracy in layer-to-layer form [2]. AM method has several types including Stereolithography (SLA) [3], Selective Laser Sintering (SLS) [4], Fused Deposition Modelling (FDM) [5], Selective Laser Melting (SLM) [6], and Direct Laser Metal Deposition (DLMD) [4], the method which is used in this study. In so many cases, there is no need to machining step as a post-process after manufacturing, and it leads to reduce the cost of production and the waste material and also increase the production time. These benefits caused AM methods to be taken into consideration and are widely studied in nowadays edge of knowledge in manufacturing technologies [7].

Direct Laser Metal Deposition (DLMD) is a type of laser-based additive manufacturing method for metals, in which the metal powder flow is applied simultaneously and melted by focusing the coaxial laser beam [8]. Figure 1 shows a schematic of the DLMD process. As shown in Fig. 1, in this method a relatively high-power laser is used to create a melt pool on the substrate surface in a neutral atmospheric environment (e.g., argon), and, the powder stream is melted with the coaxial laser beam and deposited on the substrate. The coated layers are added on each other in a pattern that is designed based on a CAD model to create the desired shape of the part [9]. In the other method for DLMD, a wire plays the role of feedstock. Abioye et al. [10] studied on DLMD with wire feedstock. They compared the wire and powder feedstock of Inconel 625. They found that powder feeding system has a wider process window for depositing continuous single tracks. However, the wire feeding system produces continuous single tracks of better surface quality and higher dimensional accuracy. In the other study [11], they evaluated the electrochemical corrosion behavior of DLMD of Inconel 625 with wire feedstock. Abioye et al. [12] used AISI 308LSi wire for laser deposition of single tracks and multiple tracks (walls) on the AISI 304 substrate.

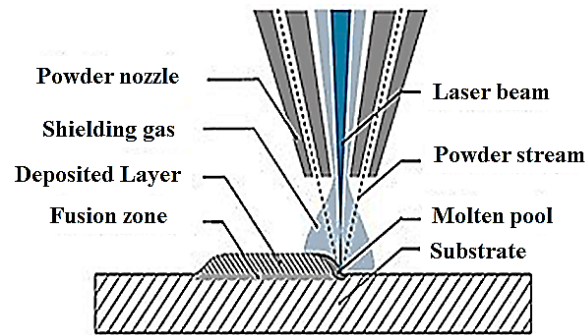


Figure 1: Schematic of the Direct Laser Metal Deposition (DLMD) process

Direct laser metal deposition technology has several advantages such as: using in a wide range of engineering materials, high cooling rates in depositing process that caused a fine-grained microstructure, near-net and net-shape capabilities, powders can be mixed for an alloying and producing functionally graded parts, controllable heat input with minimal dilution, minimal heat effect zones and the residual stresses and distortion [13]. DLMD process is also used to reduce manufacturing and remanufacturing costs, and in so many cases for repairing technologies is applied. DLMD technology is used in the fields of aerospace, medicine, military, and commercial, and it is an appropriate process for repairing and maintaining valuable components [14].

So many studies applied different metal powders such as Inconels, Stellites, Stainless steels, Titanium alloys, etc. to produce parts by DLMD. Stellite 6 superalloy is the most widely used of the wear resistant cobalt based alloys and exhibits good all-round performance. It is regarded as the industry standard for general-purpose wear resistance applications, has excellent resistance to many forms of mechanical and chemical degradation over a wide temperature range, and retains a reasonable level of hardness up to 500°C. It also has good resistance to impact and cavitation erosion. Stellite 6 is ideally suited to a variety of hard facing processes and can be turned with carbide tooling. Examples include valve seats and gates; pump shafts and bearings, erosion shields and rolling couples [15]. Marshall et al. [16] investigated the microstructure of direct laser deposition to create Ti-6Al-4V cylinders via in-situ thermal monitoring. DLMD was used to manufacture the metal matrix composites of nickel and Titanium-based alloys with variable content, structure, and properties. They found that the formation of intermetallic reinforced binary and ternary structures occurred by the phase transformations and crystallization of the alloy [17]. Foster et al. [18] worked on the Cobalt-based Stellite 21. They used the DLMD method to repair and remanufacturing of forging dies. They found that the stellite 21 DLMD additive layer performed better wear resistance properties than H13 tools steel dies. In another study, the Laser Engineered Forming (LENSTM) was performed for the production of structures with the variable combination of vanadium carbide (VC) and stainless steel

304 (SS304). The 100% VC outer layer, compared to the SS304, increased the hardness by 1,450 vices and reduced the wear rate by 95% [19].

Experimental researches reported that there are a lot of variable parameters in the DLMD process that could influence the mechanical and metallurgical properties of the additive manufactured (AMed) parts. Some of those parameters were laser beam power, scanning speed, scanning strategy, hatch distance, and thickness of the powder layer [20, 21]. Zhang et al. [22] utilized a relatively slow scanning velocity to obtain a defect-free Al-Cu-Mg alloy successfully. In another research study of LMD of 5087 Aluminum alloy, it is observed that pre-heating of the substrate turned out to be beneficial in terms of the reduction of porosity and cracking [23]. Different effects of pulsed laser parameters on direct laser deposition of Inconel 718 and Ti-6Al-4V materials were investigated. The experimental and modeling results showed that powder mass flow plays an essential role in the crack propagation during Inconel 718 and Ti-6Al-4V deposition, and it should be reduced to minimize cracking in samples [24]. In the other study, C.Y. Kong worked on the DLMD of Inconel 718 nickel-based superalloy. They realized that low heat input and high rate deposition caused only small and scattered porosity with no cracking in samples [25]. Kempen et al. worked on the optimization process and improvement of AlSi10Mg aluminum alloy parts produced by laser melting decomposition based on co-axial powder feed to improve production quality. They found that the relative density of block samples without large cavities and cracks increased to 99.2% after optimization of the process [26]. Metel et al. tried to control and improve the laser power density by Applying an additional laser beam modulator. The installation of an additional laser beam modulator increased the process efficiency [27]. The effect of laser power on the metallurgical characteristics in the DLMD process was investigated by Choo et al. [28]. They found that, when laser power decreased, the porosity linearly increased from 0.13 to 0.88%.

Directed laser deposition AM has become a promising method for fabricating parts from Stellite 6 powder [29]. The performance of St 6 components produced by laser metal deposition has been investigated by many authors in recent years. In laser metal deposition of Co-based superalloys, the laser surface melting, followed by rapid solidification of the melted layer, can develop high refined microstructures with unusual microstructures and undesirable phases [30]. Heating and cooling behavior of laser additive manufacturing are effective on creating and distributing mechanism of carbides of Cobalt-based superalloys that can change the microstructural and mechanical properties [31]. In laser additive manufacturing process of Stellite 6, significant stresses can develop due to the high thermal gradients produced by the thermal processes, high cooling, and the brittleness, all of which can sometimes lead to undesirable distortions or the appearance of cracks [32].

In spite of the efforts of these, and other researchers, many aspects of direct laser metal deposition additive manufacturing which is a new revolution in manufacturing industries is still unsolved and more research needs to be performed. Considering the variation of the location of the laser beam in the powder stream and investigating the geometrical stability of the additively manufactured walls, are relatively new additions to this field. In the present research, stellite 6 Cobalt-based superalloy powder was used for 3D printing via direct laser metal deposition method. The capabilities of the additive manufacturing were investigated by two strategies: (1) changing the focal position of the laser beam in the powder stream, (2) variation of the laser power in different samples. The geometrical dimensions (height and width), microhardness profile, grain size, and the microstructure of the 3D printed samples were characterized.

2. Experimental Work

2-1. Materials

Cobalt-base super-alloy stellite 6 powder with a particle size of 10 to 36 micrometers was used in this study. The substrate is DIN 1.2714 hot work tool steel (56NiCrMoV7). Table 1 shows the chemical composition of the powder and the substrate, identified by the X-ray fluorescence spectrometer (XRF) model PW1410. The moderate carbon of the substrate steel, chrome, nickel, molybdenum, and vanadium caused high impact and fatigue strength in high temperature and moderate thermal shock and wear resistance. The substrates were prepared by machining in dimensions of 80×20 mm with a thickness of 7 mm. In order to prepare the samples for DLMD process, the sample surfaces were grounded by grinding machine to have a smooth surface to decrease the samples surface roughness by 0.8 μm. Before conducting the AM experiments, by using acetone, the grease and residue on the surface of the base metal were removed and also the oxidation film was removed with stainless steel brush. Figure 2 depicts the morphology of the powder particles taken by scanning electron microscopy (SEM 3MIRA).

Table 1. Chemical composition of the stellite 6 powder and DIN 1.2714 substrate.

Element	Co	Cr	W	Fe	P	Mn	C	Si	S	Ni	Mo
Powder (wt. %)	Bal.	31	3	1.21	0.42	0.22	1.3	-	-	-	-
Substrate (wt. %)	-	1-1.2	-	Bal.	0.03	0.6-0.9	0.5-0.6	0.1-0.4	0.03	1.5-1.8	0.45-0.55

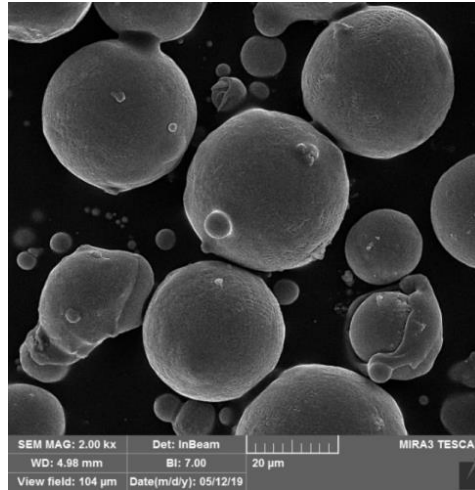


Figure 2: SEM image of stellite 6 powder particles.

2-2. Direct Laser Metal Deposition Process

To have a dense powder stream for direct laser metal deposition additive manufacturing process, a brass nozzle is used. Powder particles were blown from four powder beams channels, which are designed to focus the powder particles in the powder concentration plane (Figure 3). Different parameters such as rotating speed of the powder feeder, the axial and annular carrier argon shielding gases flow rate, standoff distance varied. In the best setting (coaxial gas flow rate = 3 lit/min and annular gas flow rate = 6 lit/min), as shown in Figure 3. The concentration zone of the powder stream was recognized 15 mm under the powder coaxial nozzle. In this powder setting, the powder flow rate was measured equal to 20 g/min.

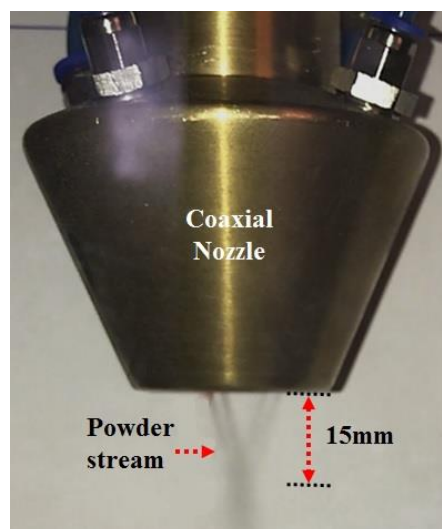


Figure 3: Powder stream and its concentration under the coaxial nozzle.

After determining the desired shape of the powder stream, the direct laser metal deposition additive manufacturing process was carried out. For the DLMD process a 1 kW Fiber laser (YFL-1000 model made in Iranian National Laser Center) with the

minimum spot size of the laser at focal position of 0.2 mm, the focal length of 200 mm, and the Rayleigh length of 2 mm was operated in continuous wave. Cobalt-base super-alloy stellite 6 powder was deposited on the DIN1.2714 hot work tool steel substrate. The length of AMed wall was 4 cm. Laser additive manufacturing experimental works were performed in two strategies, as presented in Table 2. In A series, the effects of variations of the laser focal plane position in the powder stream were surveyed in a single cladding layer. By varying this parameter, the laser energy absorption by the substrate and the stellite powder was investigated. Figure 4 illustrates the laser focal positions in different modes. The powder concentration plane is located on the surface of the substrate. As shown in Figure 4 in mode -4, the laser spot point is located 4 mm above the powder concentration plane while in +4 mode, it is located 4 mm lower down the powder concentration plane. In zero-mode, the laser spot point is positioned on the substrate and powder concentration plane.

In B series, one of the best results of A-series is selected, and the effects of changing the laser power were investigated in which each sample has 5 layers to create a wall additive manufactured. In all experiments, the scanning speed, standoff distance, and the powder flow rate were kept fixed 10 mm/s, 15 mm, and 20 g/min, respectively. In B series, after coating each layer, the CNC table moves 0.3 mm down for adding the next layer on the previous manufactured layer. The scanning pattern of adding different layers is depicted in Figure 5. During the experiments, the cooling time is set to 35 seconds per layer. Figure 6 shows the additively manufactured wall samples.

Table 2. Input parameters in the A and B series.

Strategies	Sample name	Laser Focal point position (mm)	Number of layers	Laser Power (w)
The effect of focal point position on samples (A Series)	A1	+4	1	250
	A2	+2	1	250
	A3	0	1	250
	A4	-2	1	250
	A5	-4	1	250
The effect of laser power on samples (B Series)	B1	-2	5	100
	B2	-2	5	150
	B3	-2	5	200
	B4	-2	5	250
	B5	-2	5	300

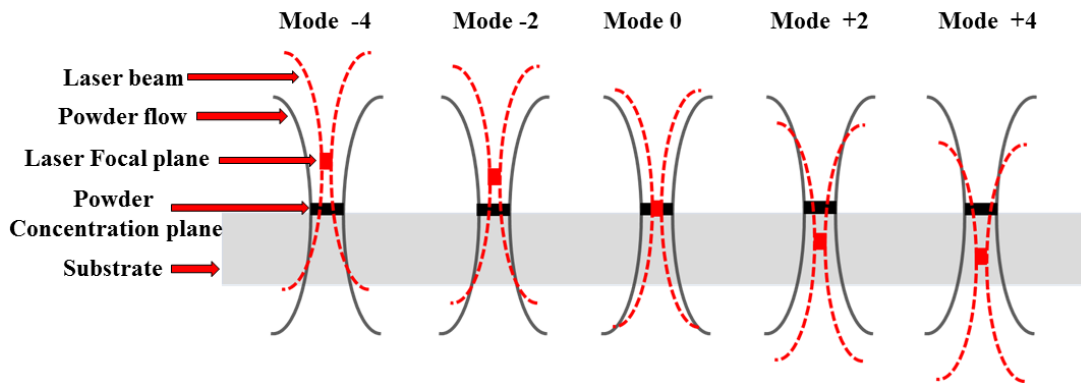


Figure 4. Variation of the laser focal plane position in the powder stream

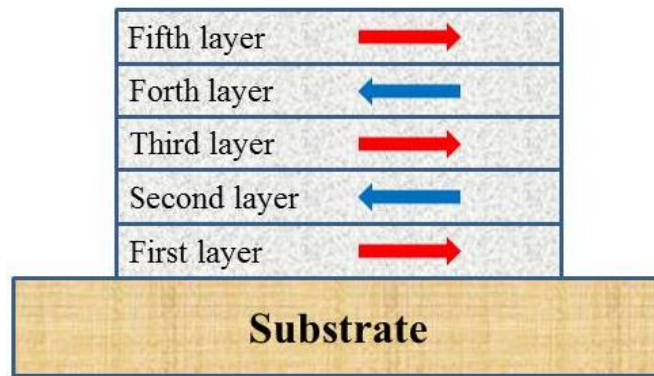


Fig. 5 The scanning pattern of the Laser Additive Manufacturing process

2-3. Characterizations

After manufacturing the specimens in two strategy series A and B, the samples were cut first from the middle and the cut specimens mounted in resin. For metallographic investigations, the samples grounded with deferent sand papers and fully polished. The polished samples have been etched in the reagent with a formula of 90 ml of HCl, 7 ml of 4SO₂H H₂SO₄, and 3 ml of 3HNO₃. OM and SEM images are taken by Kayowa optical microscope and scanning electron microscope (model LEO1455VP) for microstructure analysis. Microhardness tests were performed by using the NEXUS 4000 microhardness according to the Vickers standard along with the height of the AMed wall with a load of 500 g and dwell time of 15 seconds. Image j software was used to analyze the geometric dimensions, grains size, and geometric stability of the wall additive manufactured specimens.

3. Results and Discussion

3-1. Additive Manufactured Case Geometry

As explained in section 2-3, additive manufactured samples were prepared for characterization. Figure 6 shows the macro section of laser additive manufactured samples of A-series (single layer in upper row) and B series (5 layers in lower row). Geometrical dimensions of specimens were measured by optical microscopy and ImageJ software. Fig. 7 depicts a schematic of the additively manufactured deposited layers on the substrate. Width (W) and height (h) of the deposited wall, depth of the penetration of the layer in the substrate (d_1), and depth of the HAZ area (d_2) were measured. Table 3 shows the geometrical dimensions results of the samples. Figure 8 represent the AMed samples (A and B series).

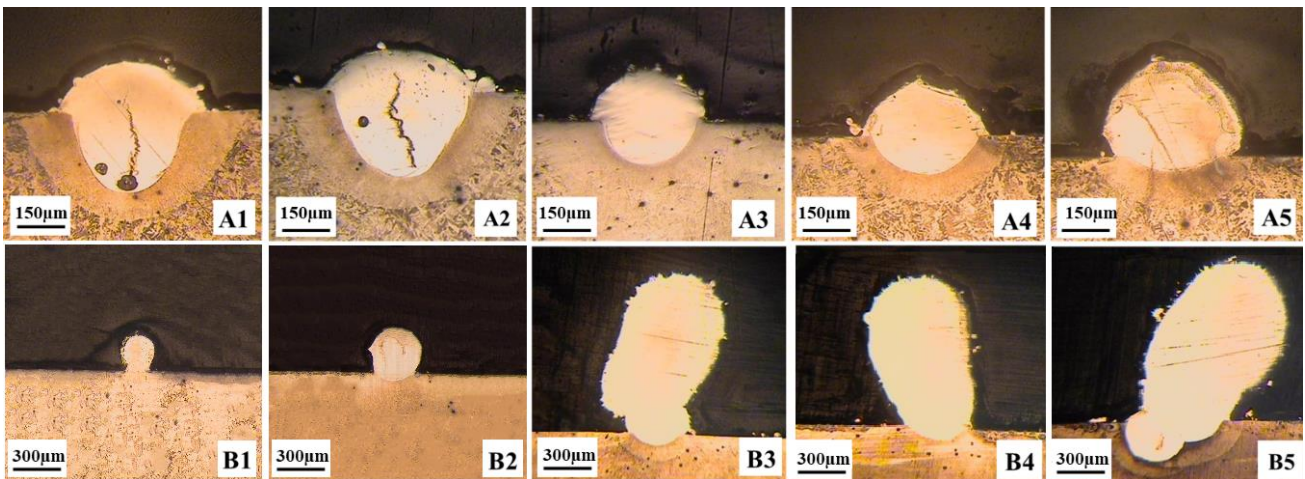


Figure 6. Macro section of laser additive manufactured samples.

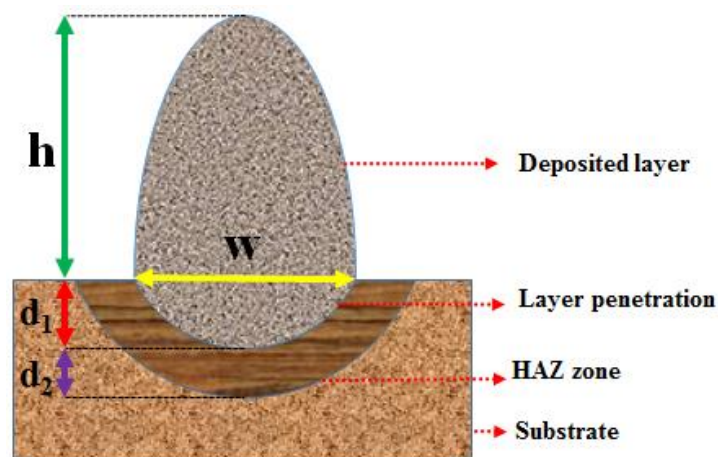


Figure 7. A schematic of the additive manufacture deposited layers on the substrate.

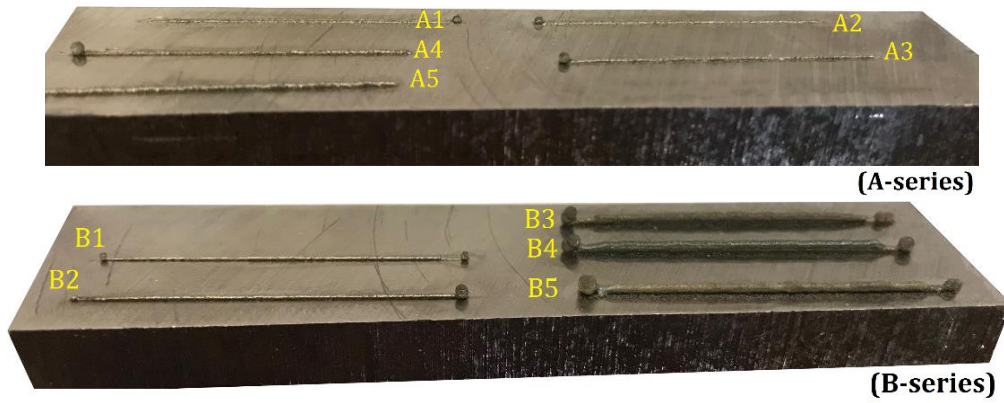


Figure 8. The images of AMed samples (the thickness of the substrate is 7 mm).

The Effects of laser beam focal plane position variations on the geometrical dimensions of the samples in A-series, single cladded layer, (presented in Fig. 7 and Table 4) of the samples are plotted in Fig. 9.

Table 3. Geometrical dimensions results of samples.

Sample name	w(μm)	h(μm)	d ₁ (μm)	d ₂ (μm)
A1	565.6	196.9	321	116.2
A2	575	154.7	343.7	126.9
A3	415.6	240.6	170.3	26.5
A4	476.5	200	153.1	117.7
A5	448.4	381.2	64.1	142.5
B1	187.5	289.4	0	0
B2	317.2	360.9	67.2	86.9
B3	435.5	1163.2	78.8	102.9
B4	507.9	1168	100.9	130.5
B5	750.7	1260.5	297.4	162.7

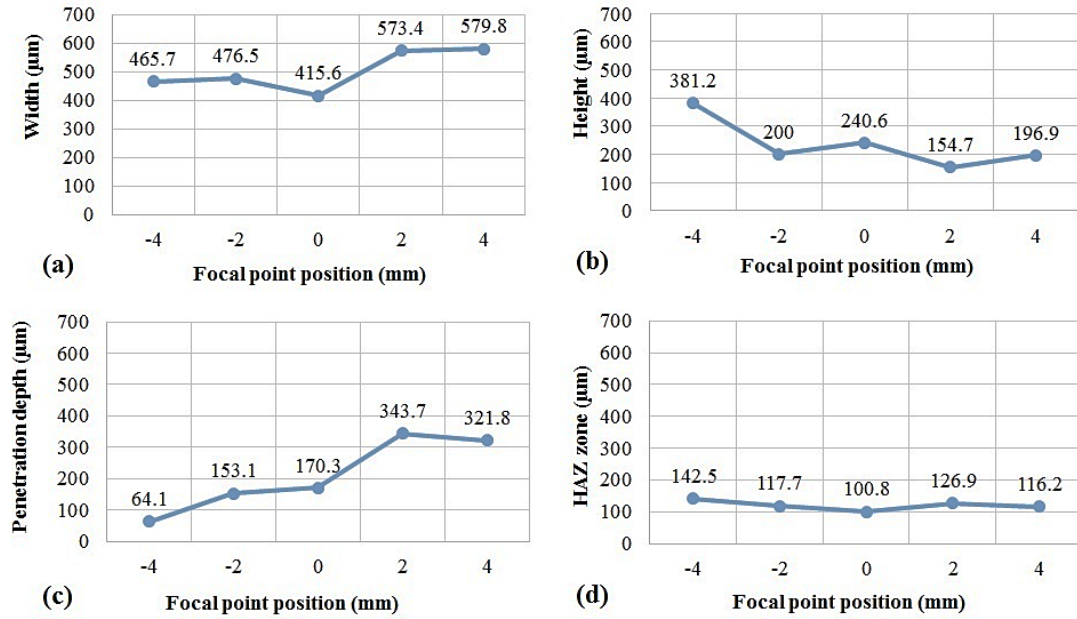


Figure 9. Effects of laser beam focal plane position variations on the geometrical dimensions of the samples in A-series (single layer) (a) width, (b) height, (c) depth of penetration in the substrate (d) HAZ thickness

See sample A1 and A2 in Fig. 6. It should be noted that, as shown by previous researches, cracking is a common defect in laser deposition process of Stellite 6 superalloy [33]. In DLMD process of Stellite 6, significant stresses developing inside the component because of the high thermal gradients induced by the thermal processes, high cooling rate resulting from a high temperature, the brittle phases at low temperatures, all of which can cause distortions and cracking. Also, the carbides may be responsible for cracking [34].

According to Table 3, the depth of the penetration of the layer in the substrate for B5 sample was the highest value. Due to the high laser power the higher depth of penetration accrued. It causes more powder to be melted as well. Also, increasing the laser power, while all other parameters kept constant and in the constant laser beam area, lead to increase the laser beam energy density. Therefore, more energy transfer to the material and the temperature will be higher, and it causes more volume of the powder to be melted and deposited on the substrate. So, during depositing the second layer, while the laser power is the same in all layers of the sample, the previous layer (1st layer) will be melted more in comparison with the other samples. It will be led to be tilted toward the substrate because of the gravity force resulting from high volume of increased molten metal that flows down the melted materials during laser deposition in different layers. And because of the high laser power, during the depositing the second layer the substrate is re-melted again. And for other layers it will be the same, which means the high laser power led to melting the previous layers. For example in depositing the 3rd layer, the 2nd and the 1st laser will be re-melted. The

second tilted layer act like a substrate for the third layer, thus the third layer was tilted as well. This trend was repeated for fourth and fifth layers. Finally, the AMed wall was not perpendicular to the substrate. It is good to mention that the tilted angle in B5 sample is more than B3 and B4 because of the higher laser power. The higher melted content caused the lower perpendicularity and lower the accurate height of the layers. In our measurements we have considered the vertical height of all samples and we did not consider the tilted wall in the measuring the height. Based on a proverb it is said that: A good beginning makes a good ending. Or in another way: All's well that ends well.

According to Fig. 9 (a), it is evidence that in mode +4 of the focal point position in which the laser focal position is below the surface, see Fig. 4, the width of the deposited layer is the largest case. Because in this mode, a wider area of the laser beam interacts with the substrate surface, and then more volume of the powder is melted and deposited on the substrate. In Fig. 9 (b), we understand that it is cleared that, when the laser beam is placed above the substrate (mode -4) while the larger laser beam area has interacted with the powder stream in comparison with the other modes, it causes more powder to be melted and create a longer height. For analyzing the penetration depth, Fig. 9 (c), it can be understand that when the laser beam focal plane moves through inside the work piece (mode -4 to +4), the penetration will be higher. The reason is the concept of the Rayleigh length of the laser beam. In mode +4 in which the focal plane position is 4 mm below the substrate surface, the length of the Rayleigh, which has the higher beam energy density, is positioned inside the substrate. So in this situation, the laser transfer more energy to the substrate and melt a larger zone. Therefore by these explanations, it can be concluded that the penetration depth will be higher. Comparing the HAZ depth in Fig. 9 (d) in the A-series specimens, it was found that the trend of the changes is very small and has almost the same values in different focal position modes.

Figure 10 illustrates the influences of laser power on the geometrical dimensions of the samples in B-series, five additively manufactured layers, presented in Fig. 7 and Table 3. By comparing the geometrical dimensions of the B-series, it can be seen that the trend of the responses is the same in laser power variations. In all diagrams in Fig. 10 by increasing the laser power dimensions will be increased. Equation 1 presents laser beam energy density:

$$\text{Laser beam energy density} = \frac{\text{laser power}}{\text{beam spot area}} \quad (1)$$

It can be concluded from Eq. 1 that increases the laser power in the constant laser beam area, the laser beam energy density increases. Therefore more energy transfer to the material and the temperature will be higher, and it causes more volume of the powder to be melted and deposited on the substrate. It caused to increase in the height

and width of the deposited layers after solidification of the melted powder [35]. In Fig. 9 c and d, it is shown that by increasing the laser power, the penetration depth and the HAZ area will be increased. It is because of the laser power enhancement which causes the increases of the heat input transfer to the substrate [36, 37].

In Fig. 10 c, it can be seen that in the B5 specimen with the power of 300 W, there was a significant increase in the depth of penetration which is not an ideal event; Because it wasted a large amount of powder by penetrating into the substrate, which is not economically feasible and energy-efficient. Also, while the depth of penetration does not play a vital role in additive manufacturing and because of the economical aspect, sample B4 can be considered a good sample among all B series from the economical aspect.

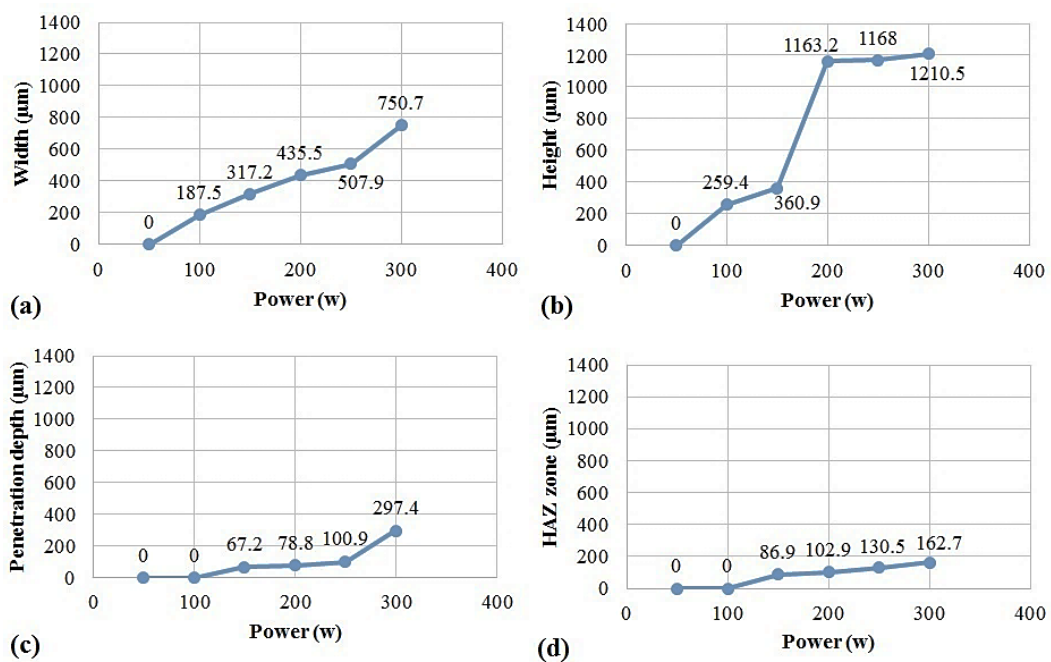


Figure 10. Effects of laser power variations on the geometrical dimensions of the samples in B series (5 layers) (a) width, (b) height, (c) depth of penetration in the substrate (d) HAZ thickness

3-2. Height Stability of AMed samples

In the additive manufacturing process, one of the important aspects of the production is to have a minimum variation in the height of the manufactured wall to be smoother and to have a higher surface quality and less distortion. The Stability of the manufactured wall is investigated to gain the mentioned purpose. From each additive manufactured sample, a photo of the manufactured wall appearance in side view was taken, as shown in Fig. 11. The wall height stability is defined through the following; the highest and lowest parts of the wall were measured at three regions, the beginning, middle, and end of the sample, as shown in Fig. 11. The length of the side view of the AMed wall sample, is divided into three equal zones as: Beginning, Middle and End

zones. The absolute height difference shows the variation of the wall height, i.e., lower difference corresponds to higher stability. In Table 4, h_1 , h_3 , and h_5 are the minimum heights and h_2 , h_4 , and h_6 are maximum heights of the AMed wall in three regions. Equations 2, 3, and 4 present the wall variation values Δh_1 , Δh_2 , and Δh_3 , respectively:

$$\Delta h_1 = h_2 - h_1 \quad (2)$$

$$\Delta h_2 = h_4 - h_3 \quad (3)$$

$$\Delta h_3 = h_6 - h_5 \quad (4)$$

The level of instability for each sample (the lower Δh , the more stable the wall) is presented by the larger of the three values:

$$\Delta H = \text{Max} \{ \Delta h_1, \Delta h_2, \Delta h_3 \} \quad (5)$$

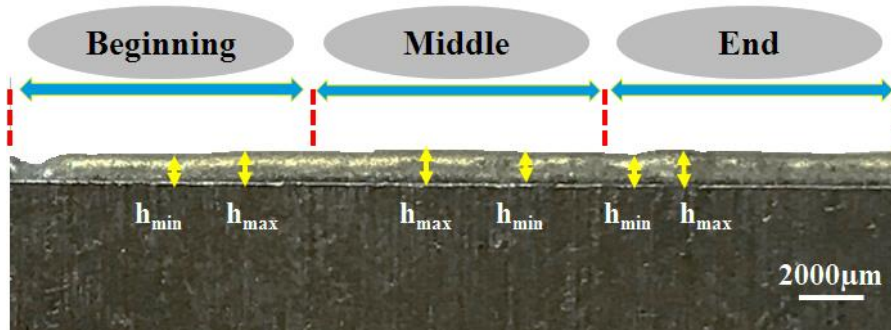


Figure 11. Additive manufactured wall height appearance and the definition of stability through three region height variation (sample B4).

Table 4. Maximum and minimum of height and differences of them in three regions (beginning, middle, and end of samples).

Sample number	h_1 (μm)	h_2 (μm)	Δh_1 (μm)	h_3 (μm)	h_4 (μm)	Δh_2 (μm)	h_5 (μm)	h_6 (μm)	Δh_3 (μm)	ΔH (μm)
B1	187.5	226.5	39	234.4	290	55.6	195.3	218.7	23.4	55.6
B2	273.4	304.6	31.2	336	375	39	289	343.7	54.7	54.7
B3	1110.3	1198.5	88.2	1404.4	1522	117.6	1242.6	1353	110.4	117.6
B4	1117.6	1220.5	102.9	1264.7	1323.5	58.8	1242.6	1308.8	66.2	102.9
B5	1000	1125	125	1150	1175	25	1150	1383	233	233

Figure 12 shows the variation of maximum height differences calculated by equation 5 (ΔH) for samples B, in which the laser power is varied, based on the values presented in Table 4. As mentioned before, in the definition in this paper, the lower the (ΔH)

causes the higher stability of the specimen [38, 39]. It is shown in Fig. 12 that the ΔH has a smooth direct trend by increasing the laser power from B1 to B5 sample (100-300 W). One of the reasons for this phenomenon can be explained by this concept that by increasing the laser power, more powder particles inside the powder stream will be melted, and also more particles may be evaporated or either sublimated. So the melted powder flow, which is down falling to the substrate surface and the previous deposited layer, will not have a steady flow. Also, by increasing the laser power, some powder particles will be spattered, which are small and unwanted droplets of molten powder emitted during the process and stick around. Thus as shown in Fig. 12 in the lower laser power, the less ΔH happen, which means more stability, better appearance, better surface quality.

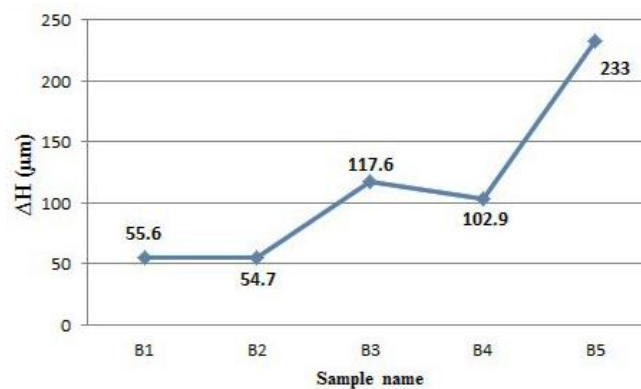


Figure 12. The maximum difference between height (ΔH) for B-series samples.

3-3. Grain size

The grain size was measured according to the Heyn method [40]. Using this method, on the metallographic images of the AMed samples, some line segments were drawn horizontally, vertically, and diagonally in five different areas, from the beginning, center, and the end of the samples. The number of grains located under each line segment was divided by line segments' length. Finally, by interpolating the grain size in these five regions, the grain size in each sample was obtained in three zones, beginning, center, and end of the sample. The grain size values in these three zones, beginning of sample (a1 and a2) center (a3 and a4) and the end (a5 and a6) for each sample are shown in Table 5. The average grain size in Table 5 show that in A series reduced from A1 to A5, and in B series the average grain size increases from B1 to B5 by increasing the laser power. The increases in the laser power lead to the higher temperature and absolutely effects on the solidification rate which is reduced. Therefore the average grain size in these samples will be higher by increasing the laser power.

Figure 13 illustrates the SEM images of the grain size changes in different areas of the AMed samples. Upper and lower pictures of Figure 13 are grain size images of A3 and B4 at the beginning, center, and end of samples, respectively. All A and B series samples have the same trend in grain size, as shown in Figure 13. Figure 14 depicts the trend diagram of the grain size changes in the three regions: beginning, center, and end of A and B series samples.

Table 5. Grain size values in three areas: beginning, center, and end of Sample for A and B series.

Sample number	a ₁ (μm)	a ₂ (μm)	a ₃ (μm)	a ₄ (μm)	a ₅ (μm)	a ₆ (μm)	Average Grain Size
A1	3.1	2.9	2.6	2.7	3.1	3.5	2.98
A2	2.5	2.4	2.1	2.3	2.6	2.7	2.43
A3	2.4	2.2	1.7	1.9	2.4	2.6	2.2
A4	2.3	2	1.8	2.1	2.6	2.7	2.25
A5	2.1	1.8	1.7	1.9	2.5	2.7	2.11
B1	2.5	2.3	1.6	1.7	2.2	2.4	2.11
B2	2.4	2.3	2.1	2.3	2.4	2.6	2.35
B3	3	2.7	2.3	2.5	2.8	3.2	2.75
B4	3.2	2.9	2.2	2.4	2.9	3.4	2.83
B5	3.4	3.2	2.6	2.8	3.3	3.5	3.13

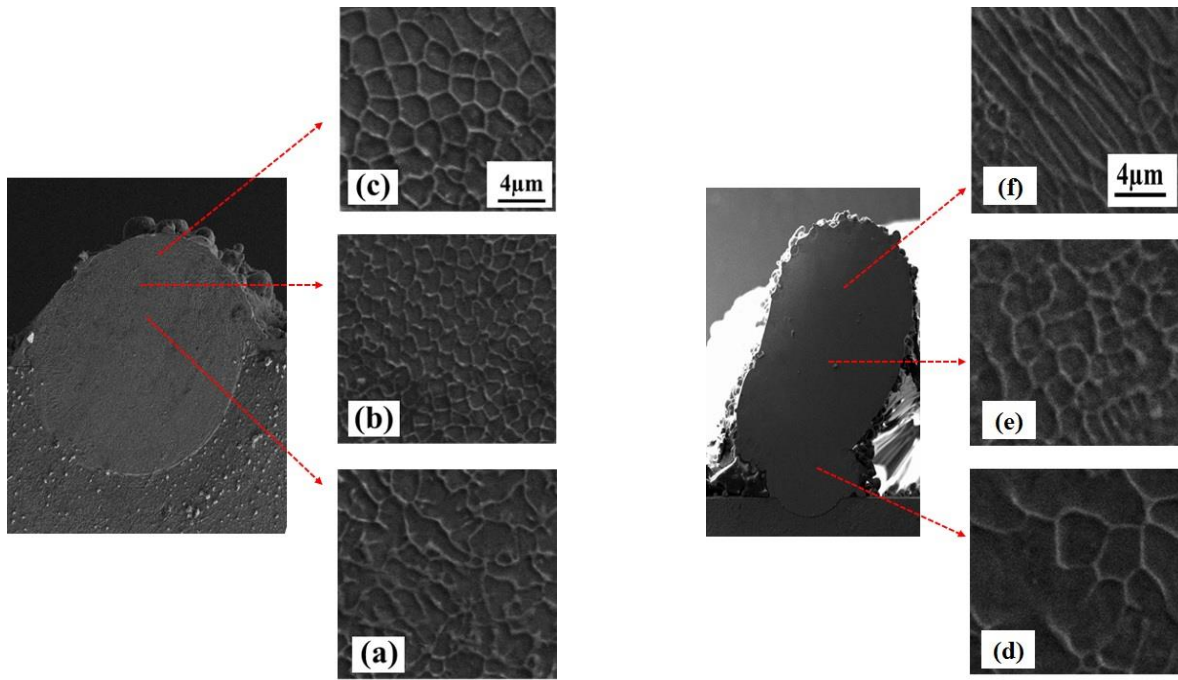


Figure 13. SEM images of grain size changes at the: (a) beginning, (b) center and (c) end of Sample A3 and at the: (d) beginning, (e) center and (f) end of sample B4

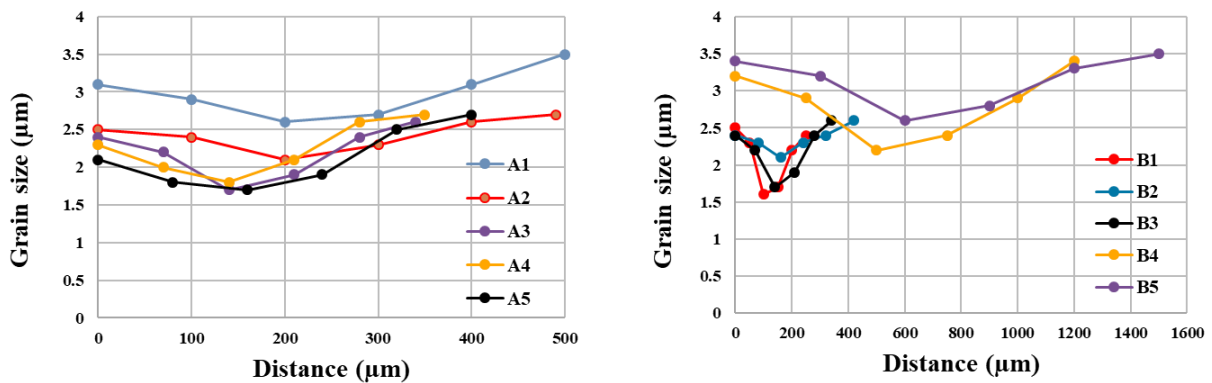


Figure 14. (a) Grain size change diagram in A-series and (b) Grain size change diagram in B-series

According to Fig 13 and 14, it was understood that the grain size, from the beginning to the center of the sample, has undergone a decreasing trend and an increasing trend from the center to the end of the sample. Also, the grain size at the center of the sample is larger than that of the beginning and end of the sample. In both A and B series, the trend of changing the grain size is the same. The reason for the larger grain size at the beginning of the deposited layer can be the higher thermal conductivity of the substrate steel ($K = 24.6 \text{ w/mk}$) than the Stellite 6 ($K = 14.82 \text{ w/mk}$) [41]. When the laser energy interacts with the powder stream on the substrate surface and both of them melted, the substrate in hears acts as a heat source and the heat inside the substrate is transferred to the layers near the substrate and led to the grain growth [42, 43]. In B-series in 5 layers deposited AMed wall, the heat temperature transfer effect will be reduced in the upper layers by getting away from the substrate surface, and the grain growth process will be reduced. In another way, it can be said that the cooling rate will be higher. In Fig. 13 and 14, it is depicted that the top layers have a larger

grain size. In addition to what has been said before, the top of the AMed layers was conducted with shielding gas and air from one side. These gases have a low heat conduction coefficient, so the absorbed heat in the end layers didn't conducted away, and remained into the layers, and it caused grain growth.

In addition to what was explained before, it is necessary to mention that, in the DLMD process, when the laser beam interacted with powder particles in the powder stream, the powder particles absorbed the laser beam energy and the laser energy attenuates. It means that the laser energy decreased little by little by absorbing with different powder particles in the powder stream. Thus a part of the laser beam energy interacts with the substrate surface and this leads to melt the substrate if the laser energy is enough. Otherwise it does not melt the substrate. In the second layer and other layers it is the same. A part of the laser that does not absorbed by the powder stream can melt the previous layer which the new layer is deposited on. So it is the main explanation of the process that leads to the melted zone in the surface and the interlayer zone which the powder is deposited. This process caused the fluctuated changes in the microstructure and grain size of those re-melted and recrystallized zones.

3-4. Microhardness

Microhardness of the AMed samples was measured by a microhardness tester device in Vickers standard, as explained in section 2-3 along the height direction of the manufactured samples. The interval of the indentation distance points are 100 μm and 200 μm in the A and B series, respectively. Microhardness distribution profile, related to the SEM cross-section images of the AMed wall in a horizontal view is shown in Figure 15. Measurements were applied in five zones including (1) substrate (2) HAZ (3) beginning (4) middle (5) and end of the deposited layer along the central axis of all manufactured wall samples for series A and B in (a) and (b), respectively. In Fig 15, each measured microhardness point in the upper profile is matched with the SEM images in the lower picture. The first point on the profile (zero point) represents microhardness value inside the substrate, and the last point represents microhardness value at the end of the sample. Also, as illustrated in Fig. 15, the height of the AMed samples can be seen in the horizontal axis.

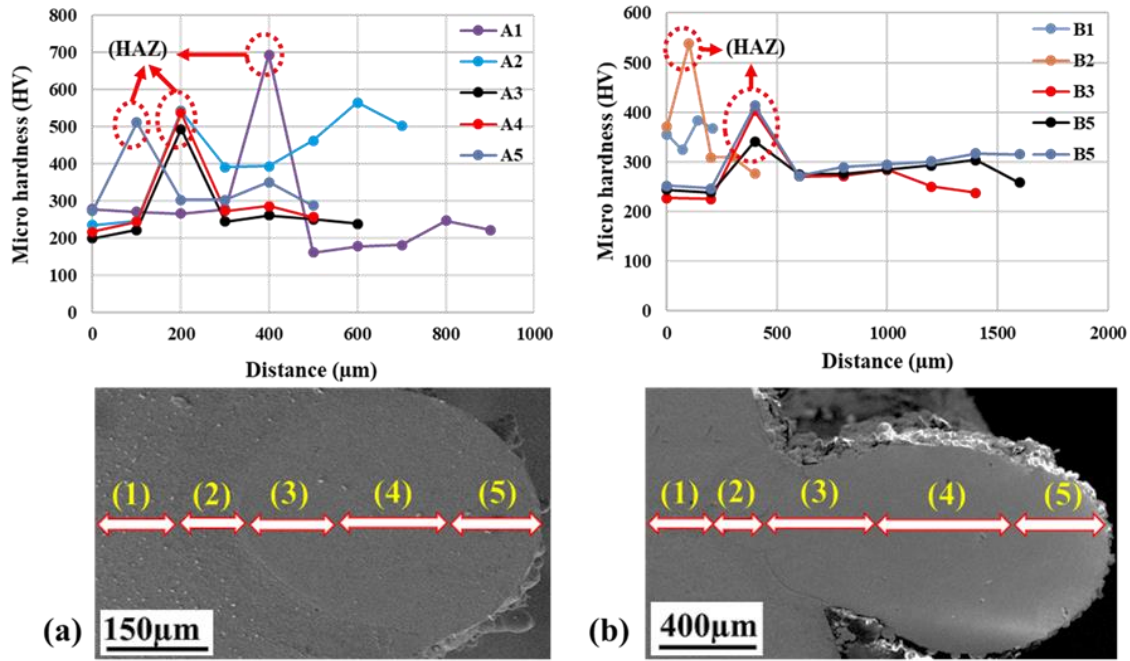


Figure 15. Microhardness distribution related to the cross-section of the AMed wall (a) A-series and (b) B-series samples.

In all microhardness diagrams shown in figure 15, there is a region in which the hardness has increased dramatically, which is the heat-affected zone (HAZ). This area is the part of the substrate in which the Stellite 6 powders are melted and mixed in the melted substrate through the laser beam and caused increases in the hardness on the steel substrate [44].

Concerning the microhardness trend of the whole sample, as shown in Fig. 15, it is clear that in A-series samples (one layer coating) and B-series (5 layers AMed), the hardness at the center of the layer is greater than that of the beginning and the end of the layer. By comparing the SEM images in Fig. 13 and the grain size distribution in Fig. 14, which were analyzed in section 3-3, with the microhardness distribution in Fig. 15, a relation between these figures can be understood. While the grain size at the center of the AMed samples is smaller than the other regions in the AMed wall, the microhardness will be higher then. On the other hand; the smaller the grain size, the higher microhardness [45-50]. Also, based on the Hall-Petch relation, equation 6, it can be shown that by decreasing the grain size, the yield strength increases, and the material strength increases [47, 48].

$$\sigma_y = \sigma_0 + Kd^{-0.5} \quad (6)$$

Where σ_y is the yield strength after the change in grain size, σ_0 is the yield strength of raw material, K is the constant coefficient of the equation, and d is the average grain diameter [44].

Furthermore, as mentioned in section 3.3, the re-melting and recrystallizing of the previous layer by the laser beam in adding the new layer, leads to changes in microstructure of the interlayer as well. Also those changes caused fluctuation in the microhardness. See Figure 15 for fluctuation in microhardness. Also fluctuation in grain size is evidence in Figure 14 which confirm the trend of Figure 15.

4. Conclusion

In this paper, the effect of the location of the focal plane position in powder stream and the laser power on the process of direct laser metal deposition additive manufacturing of stellite 6 powder was investigated. Therefore, according to the experiments, the following results can be drawn:

- 1- Changing the focal plane position of the laser beam in the powder stream has a significant effect on the metal deposited quality. When the FPP is above the substrate, the laser beam has more interaction area with the powder stream, thus the height of the AMed wall will be the highest.
- 2- Reduction the distance between the laser spot point and the powder concentration plane, leads to more height stability. Locating the laser spot point 2 mm above the powder concentration plane, has the best stability in this study.
- 3- Increases the laser power leads to increase in the width and height, but causes the lower the height stability of the AMed samples and a tilted wall. The highest stability was observed in the laser power of 100 and 150 Watts.
- 4- The grain size in the beginning and the end of the AMed wall samples are larger than the sample's center, which is related to the temperature and solidification rate inside the melt pool in metal deposition process. The higher melt pool temperature lead to the larger grain size.
- 5- The average grain size will be increased when the laser power increases. The largest and the smallest average grain size are 3.13 μm and 2.11 μm for the highest and the lowest laser power, respectively.
- 6- The trend of the microhardness changes is in reverse regime of the grain size. The smaller the grain size caused the higher microhardness. The microhardness in the center of the sample was higher than the beginning and end of the AMed wall samples.

References:

- [1]. T. D. Ngoa, A. Kashania, G. Imbalzanoa, K. T.Q. Nguyena, D. Huib, (2018), Additive manufacturing (3D printing): A review of materials, methods, applications and challenges. *Composites Part B* (143), 172–196.
- [2]. J. C. Najmon, S. Raeisi, A. Tovar, Review of additive manufacturing technologies and applications in the aerospace industry, (2019), *Additive Manufacturing for the Aerospace Industry*, 7-31.
- [3]. H. Bikas, P. Stavropoulos, G. Chryssolouris, (2016). Additive manufacturing methods and modeling approaches: a critical review. *Advanced Manufacturing Technology*, 83(1-4), 389-405.
- [4]. D. Clark, M. T.Whittaker, M. R.Bache, (2012). Microstructural characterization of a prototype titanium alloy structure processed via direct laser deposition (DLD). *Metallurgical and Materials Transactions B*, 43(2), 388-396.
- [5]. M. Moradi, S. Meiabadi, A. Kaplan, (2019). 3D Printed Parts with Honeycomb Internal Pattern by Fused Deposition Modelling; Experimental Characterization and Production Optimization. *Metals and Materials International* 25 (5), 1312-1325.
- [6]. Y. Yang, Dongdong Gu, D. Dai, C. Ma, (2018). Laser energy absorption behavior of powder particles using ray tracing method during selective laser melting additive manufacturing of aluminum alloy, *Materials & Design*, 143, 12-19.
- [7]. I. F.Ituarte, N. Boddetib, V. Hassanib, M. L. Dunnb, D. W. Rosenb,(2019), Design and additive manufacture of functionally graded structures based on digital materials, *Additive Manufacturing*, 30, 100839.
- [8]. S. M. Thompson, L. Bian, N. Shamsaei, A. Yadollahi, (2015), An Overview of Direct Laser Deposition for Additive Manufacturing Part I: Transport Phenomena, Modeling and Diagnostics, *Additive Manufacturing*, 8, 36-62.
- [9]. N. Shamsaeia, A. Yadollahia, L. Bianc, S. M. Thompsona, (2015), An overview of Direct Laser Deposition for additive manufacturing; Part II: Mechanical behavior, process parameter optimization and control, *Additive Manufacturing*, 8, 12-35.
- [10]. T.E. Abioye, P. K. Farayibi, A.T. Clare, (2017), A Comparative Study of Inconel 625 Laser Cladding by Wire and Powder Feedstock, *Materials and Manufacturing Processes*, 32(14), 1653-1659.
- [11]. T.E. Abioye, D.G. McCartney, A.T. Clarea, (2017), Laser cladding of Inconel 625 wire for corrosion protection, *Materials Processing Technology*, 217, 232–240.
- [12]. T. E. Abioye, A. Medrano-Tellez, P. K. Farayibi, P. K. Oke,(2017), Laser Metal Deposition of Multi-Track Walls of 308LSi Stainless Steel, *Materials and Manufacturing Processes*, 32(14), 1660-1666.
- [13]. P. Ghosal, M. C. Majumder, A. Chattopadhyay, (2017), Study on direct laser metal deposition, *materials today: processing*, 5, 12509-12518.
- [14]. Igor Shishkovsky, (2018), *Additive Manufacturing of High-performance Metals and Alloys - Modeling and Optimization*, chapter 4: Theory and Technology of Direct Laser Deposition.

- [15]. A. A. Pauzi, Sh. Husin, (2014), Study on the Effect of Wear Resistant Materials Applications in Reducing Wear Damage of Gas Turbine Combustor Components, *Applied Mechanics and Materials*, 575, 17-21.
- [16]. G. J.Marshall, W. J.Young, S. M.Thompson, N. Shamsaei, S. Daniewicz, S. Shao, (2016). Understanding the microstructure formation of Ti-6Al-4V during direct laser deposition via in-situ thermal monitoring, *Jom*, 68(3), 778-790.
- [17]. I. Shishkovsky, F. Missemme, I. Smurov, (2018). Metal matrix composites with ternary intermetallic inclusions fabricated by laser direct energy deposition, *Composite Structures*, 183, 663-670.
- [18]. J. Foster, C. Cullen, S Fitzpatrick, G Payne, L. Hall, J. Marashi. (2019). Remanufacture of hot forging tools and dies using laser metal deposition with powder and a hard-facing alloy Stellite 21, *Remanufacturing*, (9),189–203.
- [19]. T. Gualtieri, A. Bandyopadhyay, (2018). Additive manufacturing of compositionally gradient metal-ceramic structures: stainless steel to vanadium carbide, *Materials & Design*, 139, 419-428.
- [20]. F. Caiazzo, A. Caggiano, (2018), Laser Direct Metal Deposition of 2024 Al Alloy: Trace Geometry Prediction via Machine Learning, *Materials*, 11 (3): 444, 11030444.
- [21]. V. Zhukov, A. Ziatdinov, M. Zhukov, I. Schulz, N. Kovalchuk, S. Dubkova, Y. Korsmik, R. Klimova-Korsmik, O. Turichin, G. Perminov, A., (2019), Inconel 625/TiB₂ Metal Matrix Composites by Direct Laser Deposition, *Metals*, 9, 141.
- [22] H. Zhang, H. Zhu, T. Qi, Z. Hu, X. Zeng, (2016). Selective laser melting of high strength Al-Cu-Mg alloys: Processing, microstructure and mechanical properties, *Materials Science and Engineering: A*, 656, 47-54.
- [23] M. Froenda, S. Riekehrb, N. Kashaevb, B. Klusemannab, J. Enzb, Process development for wire-based laser metal deposition of 5087 aluminium alloy by using fibre laser, (2018), *Manufacturing Processes* (34) 721–732.
- [24]. K. Shah, H. Khurshid, I. ul Haq, S. Anwar, S. Ali Shah, (2018). Numerical modelling of pulsed and continuous wave direct laser deposition of Ti-6Al-4V and Inconel 718, *Advanced Manufacturing Technology*, 95(1-4), 847-860.
- [25]. C Y Kong, R.J Scudamore, J Allen, (2010). High-rate laser metal deposition of Inconel 718 component using low heat-input approach, *Physics Procedia* 5, 379–386.
- [26]. K. Kempen, L. Thijs, E. Yasa, M. Badrossamay, W. Verheecke, J. P. Kruth,(2011), Process Optimization and Microstructural Analysis for Selective Laser Melting of AlSi10Mg, *Conference: Solid Freeform Fabrication Symposium, At Texas, USA, Volume: 22*.
- [27]. A. S.Metel, M. M.Stebulyanin, S. V.Fedorov, A. A.Okunkova, (2019), Power Density Distribution for Laser Additive Manufacturing (SLM): Potential, Fundamentals and Advanced Applications, *Technologies*, 7, 5, 7010005.
- [28]. H. Choo, K. Sham, J. Bohling, A. Ngo, X. Xiao, Y. Ren, P. J.Depond, M. J.Matthews, E. Garlea, (2018). Effect of laser power on defect, texture, and microstructure of a laser powder bed fusion processed 316L stainless steel, *Materials & Design*, vol. 164, 107534.

- [29]. P. Muller, P. Mognol, J. Y. Hascoet, (2013). Modeling and control of a direct laser powder deposition process for functionally graded materials (FGM) parts manufacturing, *Materials Processing Technology*, Vol. 213, 685-692.
- [30]. K.C. Atony, A.N. Antony, K.J. Bhansali, (1983). Hardfacing, *ASM Handbook*, volume 6, 771–773.
- [31]. W. Gui, H. Zhang, M. Yang, T. Jin, X. Sun, and Q. Zheng, (2017). The investigation of carbides evolution in a Cobalt-base superalloy at elevated temperature, *Alloys and Compounds*, Vol. 695, 1271-1278.
- [32] G.L. Goswami, Santosh Kumar, R. Galun, B.L. Mordike, (2003). Laser cladding of Nickel based hardfacing materials as an alternative of Stellite, *BARC, Newsletter* 249, 64.
- [33]. F. Luo, A. Cockburn, R. Lupio, M. Sparkes, W. O'Neill, (2012). Performance comparison of Stellite 6 deposited on steel using supersonic laser deposition and laser cladding, *Surface and coatings technology*, vol. 212, 119-127.
- [34]. L. Fang, L. Rocco, C. Andrew, S. Martin, O. William, Y. Jian-hua, (2013). Characteristics of Stellite 6 Deposited by supersonic laser deposition under optimized parameters, *Iron and steel research, International*, 20 (2), 52-57.
- [35]. F. Lv, L. Shen, H. Liang, D. Xie, C. Wang, Z. Tian, (2019). Mechanical properties of AlSi10Mg alloy fabricated by laser melting deposition and improvements via heat treatment, *Optik*, 179, 8-18.
- [36]. G. Scotti, V. Matilainen, P. Kanninen, H. Piili, A. Salminen, T. Kallio, S. Franssila, (2014). Laser additive manufacturing of stainless steel micro fuel cells, *Power Sources*, 272, 356-361.
- [37]. Q. Wang, S. Zhang, C. H. Zhang, C. L. Wu, L. Ren, J. Q. Wang, J. Chen, (2018). Functionally Graded Stainless Steel Fabricated by Direct Laser Deposition: Anisotropy of Mechanical Properties and Hardness, *Acta Metallurgica Sinica*, 31(1), 19-26.
- [38]. B. Ren, M. Zhang, C. Chen, X. Wang, T. Zou, Z. Hu, (2017). Effect of heat treatment on microstructure and mechanical properties of stellite 12 fabricated by Laser additive manufacturing, *Materials Engineering and Performance*, 26(11), 5404-5413.
- [39]. Y. Yao, Y. Huang, B. Chen, C. Tan, Y. Su, J. Feng, (2018). Influence of processing parameters and heat treatment on the mechanical properties of 18Ni300 manufactured by laser based directed energy deposition, *Optics & Laser Technology*, 105, 171-179.
- [40] Active Standard ASTM E112, *Standard Test Methods for Determining Average Grain Size*, (2004).
- [41]. M. Moradi, M. Karami Moghadam, (2019). High power diode laser surface hardening of AISI 4130; statistical modelling and optimization, *Optics & Laser Technology*, 111, 554-570.
- [42]. M. Moradi, M. Ghoreishi, J. Frostevarg, A. F. Kaplan, (2013). An investigation on stability of laser hybrid arc welding, *Optics and Lasers in Engineering*, 51(4), 481-487.

- [43]. X. Zhan, C. Qi, Z. Gao, D. Tian, Z. Wang, (2019). The influence of heat input on microstructure and porosity during laser cladding of Invar alloy, *Optics & Laser Technology*, 113, 453-461.
- [44]. P. Asghari-Rad, P. Sathiyamoorthi, J. W.Bae, J. Moon, J. M.Park, A. Zargaran, H. S.Kim, (2019). Effect of grain size on the tensile behavior of V10Cr15Mn5Fe35Co10Ni25 high entropy alloy, *Materials Science and Engineering: A*, 744, 610-617.
- [45]. S. Kang, J. G.Jung, M. Kang, W. Woo, Y. K. Lee, (2016). The effects of grain size on yielding, strain hardening, and mechanical twinning in Fe–18Mn–0.6 C–1.5 Al twinning-induced plasticity steel, *Materials Science and Engineering: A*, 652, 212-220.
- [46]. M. Lashani Zand, B. Niroumand, A. Maleki, (2019). Determination of the Modified Hall-Petch Equation Constants and the Relationship Between the Microstructure and Mechanical Properties of AS7U3G Alloy, *Advanced Materials in Engineering*, 37(4), 91-100.
- [47]. D. Klarstrom, J. Wu, (2004). *Metallography and microstructures of cobalt and cobalt alloys*. Materials Park, OH: ASM International, 762-774.
- [48]. *Metallography and Microstructures: ASM Handbook, Volume 9*.
- [49]. F. Yan, W. Xiong, E. J. Faierson, (2017). Grain structure control of additively manufactured metallic materials, *materials*, 10, 10111260.
- [50]. J.S. Zuback, T. DebRoy, (2018). The hardness of additively manufactured alloys, *Materials*, 11, 11112070.